Proceedings of ASME 2015 Dynamic Systems and Control Conference
DSCC 2015
October 28-30, 2015, Ohio, USA

DSCC2015 - 9747

AN MPC ALGORITHM WITH COMBINED SPEED AND STEERING CONTROL FOR OBSTACLE AVOIDANCE IN AUTONOMOUS GROUND VEHICLES

Jiechao Liu
Department of Mechanical Engineering
University of Michigan
Ann Arbor, Michigan, 48109
Email: ljch@umich.edu

Paramsothy Jayakumar
U.S. Army RDECOM-TARDEC
Warren, Michigan, 48397
Email: paramsothy.jayakumar.civ@mail.mil

Jeffrey L. Stein
Department of Mechanical Engineering
University of Michigan
Ann Arbor, Michigan, 48109
Email: stein@umich.edu

Tulga Ersal*
Department of Mechanical Engineering
University of Michigan
Ann Arbor, Michigan, 48109
Email: tersal@umich.edu

ABSTRACT

This article presents a model predictive control based obstacle avoidance algorithm for autonomous ground vehicles in unstructured environments. The novelty of the algorithm is the simultaneous optimization of speed and steering without a priori knowledge about the obstacles. Obstacles are detected using a planar LIDAR sensor and a multi-phase optimal control problem is formulated to optimize the speed and steering commands within the detection range. Acceleration capability of the vehicle as a function of speed, and stability and handling concerns such as tire lift-off are taken into account as constraints in the optimization problem, whereas the cost function is formulated to navigate the vehicle as quickly as possible with smooth control commands. Thus, a safe and quick navigation is enabled without the need for a preloaded map of the environment. Simulation results show that the proposed algorithm is capable of navigating the vehicle through obstacle fields that cannot be cleared with steering control alone.

*Address all correspondence to this author.

1 INTRODUCTION

Obstacle avoidance is a critical capability for autonomous ground vehicles (AGVs). It refers to the task of sensing the vehicle's surroundings and generating control commands to navigate the vehicle safely around the obstacles. Typically, safety is interpreted as collision free, which may be an adequate interpretation in certain applications such as small ground robots. However, for the AGVs that are at least the size of a passenger vehicle, vehicle dynamics related safety concerns such as excessive sideslip or tire lift-off are also important. Thus, obstacle avoidance algorithms are needed that can utilize knowledge of vehicle dynamics to avoid collisions even when the vehicle is operated at its limits. Creating such algorithms would not only be beneficial for safe and fast navigation of AGVs, thereby improving their performance, but they could also be used as an advanced safety feature in human driven vehicles.

Many obstacle avoidance algorithms have been developed in the literature that allow for fast, continuous, and smooth motion of AGVs among unexpected obstacles. The can be classified into four categories: graph search based methods [1] [2], virtual potential and navigation function based methods [3] [4], meta-heuristic based methods [5], and mathematical

Report Documentation Page

Form Approved
OMB No. 0704-0188

1. REPORT DATE	2. REPORT TYPE	3. DATES COVERED
24 APR 2015		**00-00-2015 to 00-00-2015**

4. TITLE AND SUBTITLE	5a. CONTRACT NUMBER
An MPC Algorithm with Combined Speed and Steering Control for Obstacle Avoidance in Autonomous Ground Vehicles	5b. GRANT NUMBER
	5c. PROGRAM ELEMENT NUMBER
6. AUTHOR(S)	5d. PROJECT NUMBER
	5e. TASK NUMBER
	5f. WORK UNIT NUMBER
7. PERFORMING ORGANIZATION NAME(S) AND ADDRESS(ES) **US Army RDECOM-TARDEC,6501 E. 11 Mile Road,Warren,MI,48397-5000**	8. PERFORMING ORGANIZATION REPORT NUMBER
9. SPONSORING/MONITORING AGENCY NAME(S) AND ADDRESS(ES)	10. SPONSOR/MONITOR'S ACRONYM(S)
	11. SPONSOR/MONITOR'S REPORT NUMBER(S)

12. DISTRIBUTION/AVAILABILITY STATEMENT
Approved for public release; distribution unlimited

13. SUPPLEMENTARY NOTES
Proceedings of ASME 2015 Dynamic Systems and Control Conference, DSCC 2015, October 28-30, 2015, Ohio, USA DSCC2015-9747

14. ABSTRACT
See Report

15. SUBJECT TERMS

16. SECURITY CLASSIFICATION OF:			17. LIMITATION OF ABSTRACT	18. NUMBER OF PAGES	19a. NAME OF RESPONSIBLE PERSON
a. REPORT **unclassified**	b. ABSTRACT **unclassified**	c. THIS PAGE **unclassified**	**Same as Report (SAR)**	**9**	

optimization based methods [6] [7]. Among these categories, mathematical optimization based methods are particularly attractive, because they offer a rigorous and systematic approach to take vehicle dynamics and safety constraints into account. The model predictive control (MPC) approach is a widely adopted mathematical optimization based approach. Prior research has demonstrated successful applications of MPC to obstacle avoidance in AGVs [8], [9], [10], [11], [12], [13]. Some active safety methods leverage the MPC framework, as well, to ensure, for example, safe lane keeping or vehicle stability [14], [15], [16], [17]. The first applications of MPC to obstacle avoidance in AGVs assumed that the controller has full knowledge about the environment. They also were not concerned with the level of fidelity that the model used by the controller needs to possess for satisfactory performance, where the performance criteria in some cases also include the dynamical safety of the vehicle, such as no tire lift-off. Prior work by the authors developed a nonlinear MPC algorithm with a corresponding sensor data processing algorithm for obstacle avoidance in high-speed, large-size autonomous ground vehicles that perceive the environment only through a planar LIDAR sensor [18], [19]. The algorithm can navigate an AGV in an obstacle field without collision while ensuring vehicle dynamical safety. However, the formulation assumes that the vehicle speed is constant, which can limit the mobiltiy performance and the obstacle fields that can be cleared with this algorithm.

This paper presents a novel MPC formulation that simultaneously optimizes both the longitudinal speed and steering control commands in an AGV that relies only on a planar LIDAR sensor to detect the obstacles. A typical military truck is considered as a reprentative high-speed, large-size AGV with significant vehicle dynamics. No map of the environment is available to the algorithm, but the target location is assumed to be known. Given the obstacle boundaries that are detected within the LIDAR range and the vehicle's dynamic and mechanical constraints, the algorithm aims to navigate the vehicle as quickly as possible towards the target while ensuring safety. Vehicle dynamics are taken into account through a 3 degrees of freedom (DoF) vehicle model in the algorithm. Vehicle speed and acceleration limits are generated based on a powertrain model. For the particular vehicle of interest, the vehicle dynamical safety requirement is translated to avoiding single tire lift-off, because tire lift-off will happen before excessive sideslip. A constrained optimal control problem (OCP) is formulated and solved within the MPC framework. Simulations with a 14 DoF vehicle model as the plant are given to highlight the benefits of the new framework compared to prior work.

The rest of the paper is organized as follows. Section 2 gives an overview of the nonlinear MPC-based obstacle avoidance algorithm. Section 3 presents the OCP formulation in the MPC in detail and outlines the solution strategy. Section 4 presents and discusses the simulation results. Conclusions are drawn in Section 5.

2 OVERVIEW OF THE MPC-BASED OBSTACLE AVOIDANCE FRAMEWORK

Fig. 1 shows the schematic of the nonlinear MPC algorithm with the AGV in closed loop. This section gives an overview of this framework and explains its basic flow at a high level.

The problem of interest to be solved with the MPC framework can be summarized as follows. Consider an AGV in an unstructured environment as illustrated in Fig. 2. Here the term "unstructred environment" means that there are no lanes to follow and no traffic rules to obey. The mission of the AGV is to move from its initial position to a given goal position safely and as quickly as possible. Between the two positions there exist obstacles, whose location, size, and shape are not known *a priori*. Obstacle information is obtained through a planar LIDAR sensor, which is mounted in front of the vehicle and returns the distance to the closest obstacle boundary in each radial direction at an angular resolution of ε. Fig. 2 illustrates a case with three obstacles. The vehicle is assumed to travel on a planar surface; hence, a 2D representation as shown in Fig. 2b suffices for the purposes of this work.

The task of the MPC algorithm is to use the LIDAR data to nagivate the vehicle through the obstacle field safely

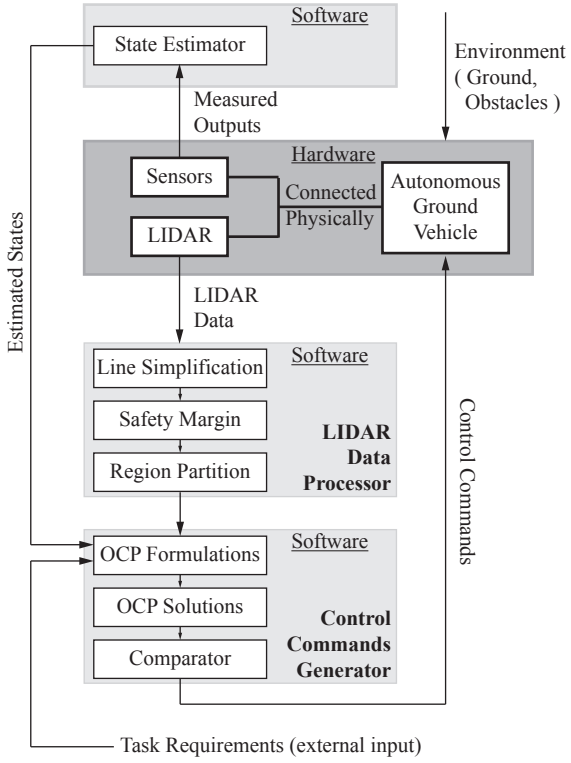

FIGURE 1. Schematic of the MPC based obstacle avoidance algorithm.

and quickly. Two safety constraints are considered; namely, avoiding the obstacles, and ensuring the vehicle's dynamical safety. The first safety constraint is fulfilled by constraining the position of the AGV inside the safe region established from the LIDAR data. The data from LIDAR is first processed by simplifying the obstacle shape and adding safety margins. As shown by the example safe region in Fig. 2b, which is the shaded area, it is typically not possible to define the safe area using a single differentiable function. This is problematic, because the OCP solver requires all functions to be twice continuously differentiable. To address this challenge, the safe region is partitioned into several sub-regions and a multi-phase OCP formulation is used. The procedures of partitioning and the usage of sub-regions are described in detail in [19]. Only the basic ideas are summarized here for brevity.

Assuming the edges of the obstacles are straight, the safe region can be partitioned in a way such that each sub-region can be specified by a set of linear inequalities. Many partitioning options exist and Fig. 3 illustrates one way of partitioning the safe region shown in Fig. 2b. In this approach, the safe area is divided into sectors and triangles, where sectors are called openings and they are free from obstacles, whereas triangles are regions terminated by obstacle boundaries. To avoid obstacles and move towards the target, the first sub-region to transverse is the sub-region in front of the vehicle (OB4), and the last sub-region to transverse is one of the openings. Note, however, that because of the limited turning radius of the vehicle, not all openings are necessarily feasible. For example, in Fig. 3, there are two feasible openings, OP2 and OP3, whereas OP1 and OP4 are infeasible opening, because the vehicle cannot steer into these sub-regions without moving outside the safe region. Thus, there are two possible sub-region sequences the vehicle can move through: OB4 $\rightarrow$ OP2 and OB4 $\rightarrow$ OP3. Based on the location of the goal position, one or both of the sub-region sequences need to be evaluated. Thus, at each step of the MPC, a multi-phase OCP is formulated for each of the sequences to be evaluated. The OCP is multi-phase because the optimal trajectory typically needs to traverse multiple sub-regions and hence the position constraints are different for each sub-region. Fig. 4 shows the optimal trajectory for the sequence OB4 $\rightarrow$ OP3 as an example. The optimal trajectory for the sequence OB4 $\rightarrow$ OP2 is obtained similarly. These two optimal trajectories are then compared and the control commands corresponding to the better one is executed by the AGV.

The second safety constraint is ensuring dynamical safety, which is defined as avoiding single tire lift-off. The details of this constraint are discussed in Section 3.

3 OPTIMAL CONTROL PROBLEM FORMULATION

This section presents the main contribution of this paper; namely, the multi-phase OCP formulation that needs to be solved at each step of the MPC to simultaneously optimize the longitudinal speed and steering angle.

The formulation in general form is given by

$$J = \mathscr{T}\left[\xi^{(N)}\left(T^N\right), \zeta^{(N)}\left(T^N\right), T^N\right]$$

$$\underset{\xi,\zeta,T^1,\ldots,T^N}{\text{minimize}} \quad + \sum_{i=1}^{N}\left\{\int_{T^{i-1}}^{T^i} \mathscr{I}\left[\xi^{(i)}(t), \zeta^{(i)}(t)\right] \mathrm{d}t\right\} \tag{1}$$

$$\underset{\forall i=1,\ldots,N}{\text{subject to}} \quad \dot{\xi}^{(i)}(t) = \mathscr{V}\left[\xi^{(i)}(t), \zeta^{(i)}(t)\right] \tag{2}$$

$$\xi^{(i)}\left(T^{i-1}\right) = \xi^{(i-1)}\left(T^{i-1}\right), \ \xi^{(0)}\left(T^0\right) = \xi_0 \tag{3}$$

$$\mathscr{R}^{(i)}\left[x^{(i)}(t), y^{(i)}(t)\right] \leq 0 \tag{4}$$

$$\mathscr{S}\left[\dot{\xi}^{(i)}(t), \xi^{(i)}(t)\right] \leq 0 \tag{5}$$

$$\delta_{f,\min} \leq \delta_f^{(i)}(t) \leq \delta_{f,\max} \tag{6}$$

$$\varsigma_{f,\min} \leq \varsigma_f^{(i)}(t) \leq \varsigma_{f,\max} \tag{7}$$

$$U_{\min} \leq U^{(i)}(t) \leq U_{\max} \tag{8}$$

$$a_{x,\min}\left[U^{(i)}(t)\right] \leq a_x^{(i)}(t) \leq a_{x,\max}\left[U^{(i)}(t)\right] \tag{9}$$

$$J_{x,\min} \leq J_x^{(i)}(t) \leq J_{x,\max} \tag{10}$$

$$U\left(T_p\right) \leq U_{\text{threshold}} \tag{11}$$

$$\sqrt{\left[x\left(T_p\right) - x(0)\right]^2 + \left[y\left(T_p\right) - y(0)\right]^2} \leq R_{\text{LIDAR}} \tag{12}$$

$$\begin{aligned} &t \in \left[T^{i-1}, T^i\right], T^{i-1} < T^i \\ &T^0 = 0, T^N = T_p, T_{p,\min} < T_p \leq T_{p,\max} \end{aligned} \tag{13}$$

By minimizing the cost function specified in Eq. (1), subject to constraints defined in Eq. (2) - Eq. (13) for all phases, the optimal state trajectories $\xi^{(i)}(t), t \in [T^{i-1}, T^i]$, the optimal control trajectories $\zeta^{(i)}(t), t \in [T^{i-1}, T^i]$, and the times T^{i-1}, T^i, $i = 1, \ldots, N$ for transitioning from one sub-region to the next are obtained, where N is the total number of phases; i.e., the number of sub-regions in a given sequence. The following sub-sections define the variables and explain the problem formulation in detail. The constraints are discussed first, and the cost function formulation is explained next.

3.1 Eq. (2): Vehicle model

A 3 DoF vehicle model is used in the MPC to predict the dynamics of the AGV. As shown in [19], this model is sufficient for the purposes of MPC when the longitudinal load transfer and tire nonlinearities are taken into account. The state-space equation for the 3 DoF nonlinear vehicle model can be written as

$$\dot{\xi} = \mathscr{A}(\xi) + \mathscr{B}\zeta \tag{14}$$

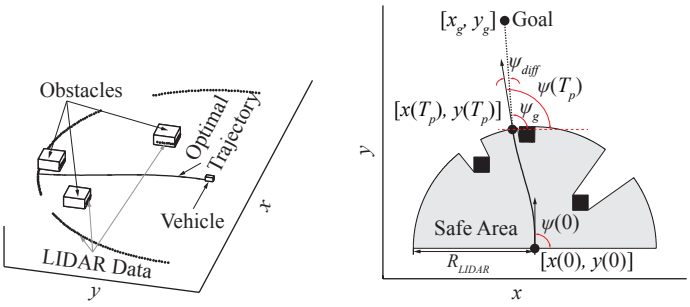

(a) A sample obstacle field and the LIDAR detection data plotted in the 3D space

(b) Top view of the LIDAR data and the safe area

FIGURE 2. A sample obstacle field and the output of LIDAR.

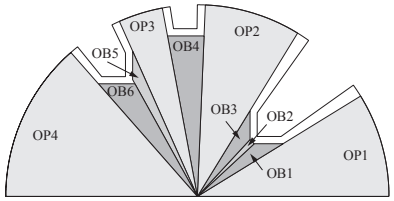

FIGURE 3. Exemplified partition of the safe region.

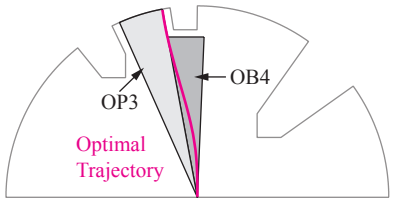

FIGURE 4. An example of sub-region sequence and the corresponding optimal trajectory.

with

$$\mathscr{A}(\xi) = \begin{bmatrix} U\cos\psi - (V + L_f r)\sin\psi \\ U\sin\psi + (V + L_f r)\cos\psi \\ r \\ a_x \\ (F_{y,f} + F_{y,r})/M - Ur \\ (F_{y,f}L_f - F_{y,r}L_r)/I_{zz} \\ 0 \\ 0 \end{bmatrix}$$

$$\mathscr{B}^T = \begin{bmatrix} 0\,0\,0\,0\,0\,0\,1\,0 \\ 0\,0\,0\,0\,0\,0\,0\,1 \end{bmatrix}$$

where the state vector is $\xi^T = [x\ y\ \psi\ U\ V\ r\ \delta_f\ a_x]$ and the control vector is $\zeta^T = [\varsigma_f\ J_x]$. As shown in Fig. 5, (x,y) is the vehicle's front center position in global coordinates; ψ is yaw angle; U, and V are longitudinal and lateral speeds in vehicle fixed coordinate, respectively; r is yaw rate; δ_f is steering angle; a_x is longitudinal acceleration; ζ_f is steering rate; and J_x is longitudinal jerk. As for the vehicle parameters, M is vehicle mass; I_{zz} is moment of inertia; and L_f and L_r are distances between the vehicle's center of gravity location and the front axle and rear axle, respectively. $F_{y,f}$ and $F_{y,r}$ are tire lateral forces generated at the front axle and the rear axle, respectively. They are predicted using the the pure-slip Pacejka Magic Formula tire model [20], and are functions of corresponding tire vertical loads and slip angles as shown in Fig. 6.

In the tire model, tire vertical loads are required as inputs. The vertical loads acting on the four wheels are given by the following equations [21]

$$F_{z,fl} = \tfrac{1}{2}\left(F_{z,f0} - \Delta F_{z,x}\right) - \Delta F_{z,yf} \quad (15)$$

$$F_{z,fr} = \tfrac{1}{2}\left(F_{z,f0} - \Delta F_{z,x}\right) + \Delta F_{z,yf} \quad (16)$$

$$F_{z,rl} = \tfrac{1}{2}\left(F_{z,r0} + \Delta F_{z,x}\right) - \Delta F_{z,yr} \quad (17)$$

$$F_{z,rr} = \tfrac{1}{2}\left(F_{z,r0} + \Delta F_{z,x}\right) + \Delta F_{z,yr} \quad (18)$$

where $F_{z,f0} = \frac{MLrg}{L_f+L_r}$ is the static front axle load; $F_{z,r0} = \frac{MLfg}{L_f+L_r}$ is the static rear axle load; $\Delta F_{z,x}$ is the longitudinal load transfer; $\Delta F_{z,yf}$ is the front axle lateral load transfer; and $\Delta F_{z,yr}$ is the rear axle lateral load transfer.

These load transfers are approximated by the following relationships

$$\Delta F_{z,x} \approx K_{z,x}\left(\dot{U} - Vr\right) \quad (19)$$

$$\Delta F_{z,yf} \approx K_{z,yf}\left(\dot{V} + Ur\right) \quad (20)$$

$$\Delta F_{z,yr} \approx K_{z,yr}\left(\dot{V} + Ur\right) \quad (21)$$

where $K_{z,x}$ is defined as the longitudinal load transfer coefficient; and $K_{z,yf}$ and $K_{z,yr}$ are defined as the front and rear lateral

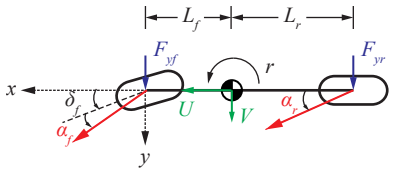

FIGURE 5. Schematic of the 3 DoF vehicle model.

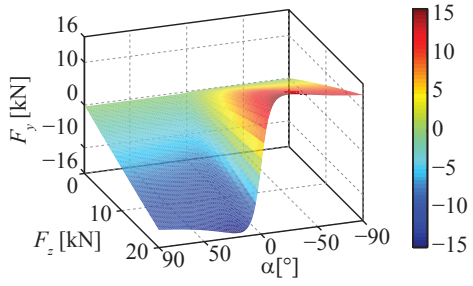

FIGURE 6. Lateral tire forces described by the Pacejka tire model.

load transfer coefficients, respectively. These coefficients are obtained from several sets of simulations with a 14 DoF vehicle model [22] that includes suspension dynamics [22], nonlinear tire dynamics [20], powertrain dynamics [23] [24], and brake dynamics [25]. The details of the complete model is omitted here for brevity, but can be found in the referred papers.

Fig. 7 and Fig. 8 show the simulation results for the longitudinal and lateral load transfers with the 14 DoF model and the straight line fittings whose slopes represent the constant load transfer coefficients.

To obtain the longitudinal load transfer coefficient, two sets of simulations are conducted. In the first set of simulations, the throttle command is maintained constant at different levels with zero braking command and zero steering angle. The results are used to study the longitudinal load transfer during vehicle acceleration. In the second set of simulations, the braking command is maintained constant at different levels with zero throttle command and zero steering angle. The results can then be used to study the longitudinal load transfer during vehicle deceleration. The black dashed line in Fig. 7 is a line that passes through the origin with a slope estimated from these two sets of data. The deviation from this line to the upper left side is caused by aerodynamic drag.

The data for estimating the lateral load transfer coefficients is generated by following the maneuver specified by Fig. 9a and Fig. 9b. The vehicle steers with a sinusoidal angle. In the meantime, the speed is changing at a slower frequency. Fig. 8 shows the simulation data points and the fitted lines. Simulations with other maneuvers confirm the results.

Even through the results from the simulations are not perfectly affine, the approximations in Eq. (19)-(21) are sufficient for the purposes of this work as the approximation error introduced by these estimated coefficients is on the order of 5% as the comparative simulation results in Fig. 9 illustrate.

3.2 Eq. (3): Initialization

The initial states of each phase are set the same as the final states of the previous phase. For the first phase, the initial values of the states x, y, ψ, V, and r are from the measurements. To maintain a smooth reference speed and a smooth steering sequence, the initial values of U, a_x, and δ_f are the values from the end of the execution horizon of the previous step.

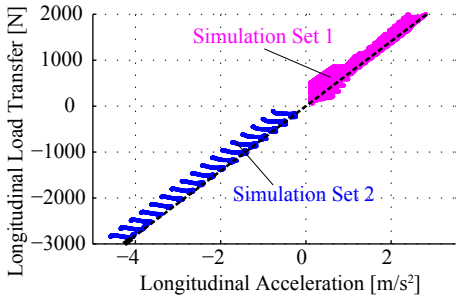

FIGURE 7. Longitudinal load transfer as a function of longitudinal acceleration.

3.3 Eq. (4): Position constraints

Vehicle obstacle avoidance is enforced through position constraints; the vehicle trajectory must stay within the safe region that is obtained after the LIDAR data is processed. For each of the phase in the OCP, a set of position constraints compacted in the following form is applied

$$A^{(i)}_{L\times 1}x^{(i)}(t) + B^{(i)}_{L\times 1}y^{(i)}(t) \leq C^{(i)}_{L\times 1}, t \in [T^{i-1}, T^{i}] \qquad (22)$$

where $A^{(i)}_{L\times 1}$, $B^{(i)}_{L\times 1}$, and $C^{(i)}_{L\times 1}$ are vectors of length L, which is the total number of lines bounding the sub-region in phase i. The

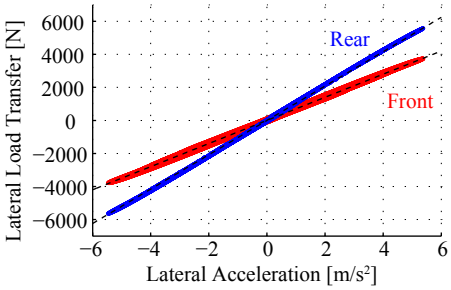

FIGURE 8. Front and rear lateral load transfers as a function of lateral acceleration, respectively.

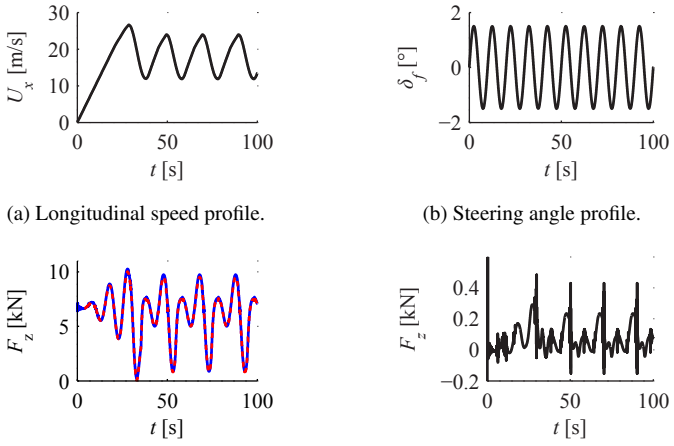

(a) Longitudinal speed profile.

(b) Steering angle profile.

(c) Comparison of the actual and the predicted vertical loads.

(d) Difference of the actual and the predicted vertical loads.

FIGURE 9. A sample simulation used to validate the accuracy of vertical load prediction. The vehicle performs the maneuver specified by subplots (a) and (b). The blue solid line in subplot (c) is the vertical load of rear left tire from the 14 DoF vehicle model. The red dashed line is the prediction using Eq. (17) with state values from the 14 DoF vehicle model simulation.

entries of these vectors are the outputs of LIDAR data processor.

3.4 Eq. (5): Dynamical safety constraints

In this study, ensuring the vehicle's dynamical safety is translated to avoiding single tire lift-off. This is a conservative criterion used to prevent rollover [26]. Prior work enforced this constraint through steering angle bounds [7], or lateral acceleration bounds [27]. However, these approaches ignore the effect of longitudinal acceleration, which is an important factor to consider in the variable speed case. Hence, in this work, the no tire lift-off requirement is taken into account directly by enforcing a positive vertical load on all four tires at all times. Because $F_{z,f0} > F_{z,r0}$ and $K_{z,yr} > K_{z,yf}$, vertical loads of the two tires on the back are constrained to be greater than a positive threshold value. In Fig. 10, the range of vehicle accelerations for limiting rear tire vertical loads is smaller than the range for limiting front tire vertical loads. Thus, it is sufficient to include only the vertical load limits of the two rear tires.

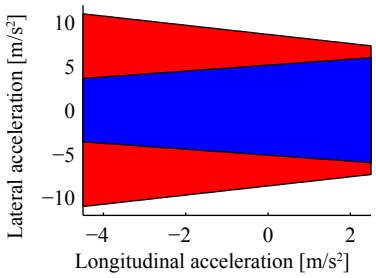

FIGURE 10. When the vehicle accelerations are within the entire colored region, the vertical loads of the two front tires will be greater than $F_{z,\text{threshold}} = 1000$ N. However, to make sure that the vertical loads of the two rear tires are greater than this threshold, the vehicle accelerations need to stay within the blue region.

This constraint can be expressed using the following inequalities, which are obtained by substituting Eq. (19), and Eq. (21) into Eq. (17), and Eq. (18):

$$\begin{aligned} &\tfrac{1}{2}\left[F_{z,r0} + K_{z,x}\left(\dot{U}^{(i)}(t) - V^{(i)}(t)r^{(i)}(t)\right)\right] \pm \\ &K_{z,yr}\left(\dot{V}^{(i)}(t) + U^{(i)}(t)r^{(i)}(t)\right) \geq F_{z,\text{threshold}} \end{aligned} \tag{23}$$

Another important vehicle dynamics related safety concern is excessive sideslip, which is considered as a handling instability. To prevent it, methods such as using a yaw-sideslip state envelope [17] could be employed. However, the vehicle platform of interest in this work has a relatively higher center of gravity and thus tire lift-off occurs before excessive sideslip.

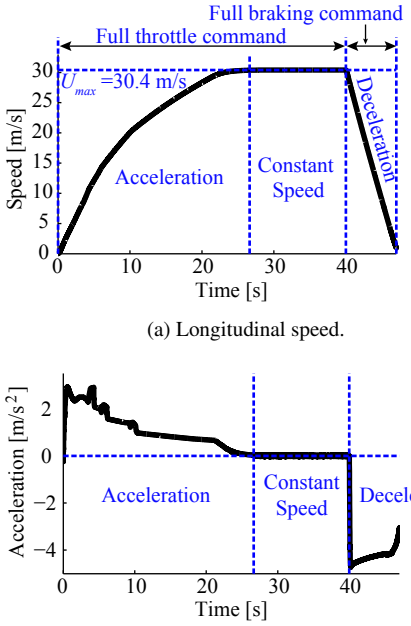

(a) Longitudinal speed.

(b) Longitudinal acceleration.

FIGURE 11. Vehicle longitudinal speed and acceleration profiles for a full throttle - full brake cycle.

3.5 Eq. (6) - Eq. (10): State and Control Bounds

Constant bounds are imposed on the steering angle and steering rate in Eq. (6), and Eq. (7), respectively. These bounds reflect the vehicle mechanical limits and steering actuator performance limits.

The vehicle speed, acceleration, jerk bounds in Eq. (8), Eq. (9), and Eq. (10) are associated with the powertrain and brake dynamics. Powertrain dynamics are modeled according to [23] [24]. The model includes the flywheel, engine, torque converter, transmission, and differential. The dynamics of the hydraulically actuated brake is modeled using the single state model in [25] that produces a good representation of the dynamics from the master cylinder to vehicle deceleration. Fig. 11a and Fig. 11b are longitudinal speed and acceleration profiles, respectively, when a full throttle command is applied followed by a full braking command. As a result of this simulation, the maximum speed is set as 30 m/s in the OCP formulation. Furthermore, as shown in Fig. 12, acceleration capability depends on the instantaneous speed. The upper bound and lower bound are approximated using fourth order polynomials as follows:

$$a_{x,\max}(U) = c_1U^3 + c_2U^2 + c_3U + c_4 \tag{24}$$

$$a_{x,\min}(U) = c_5U^3 + c_6U^2 + c_7U + c_8 \tag{25}$$

where, $c_1, \cdots, c_8$ are parameters obtained from polynomial fitting to the simulation data.

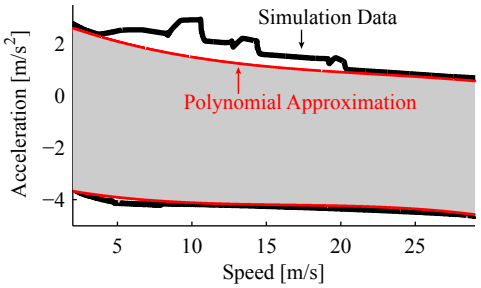

FIGURE 12. Vehicle acceleration limits as a function of vehicle longitudinal speed.

3.6 Eq. (11) - Eq. (13): Terminal constraints

The first terminal constraint, Eq. (11), limits the vehicle speed at the end of the prediction horizon. This limit is introduced to prepare for potential obstacles in the future. Specifically, the vehicle is allowed to accelerate at the beginning of the prediction horizon, but then is required to decelerate to a threshold speed at the end of the prediction horizon, since no obstacle information such as location, shape, and size are known *a priori*. The second terminal constraint, Eq. (12), constrains the vehicle trajectory to be within the LIDAR detection range. The third terminal constraint, Eq. (13), specifies the limits on the prediction horizon.

3.7 Eq. (1): Cost function

The cost function defines in what sense a trajectory is considered to be optimal. In this work, the cost function formulation includes six terms that are linearly combined using relative weights as follows:

$$J = \frac{s_T}{s_0} + w_\psi \psi_{\text{diff}}^2 + w_t T_p + w_{I_1} I_1 + w_{I_2} I_2 + w_{I_3} I_3 \tag{26}$$

where s_0 is the distance between the prediction initial position $[x(0), y(0)]$ and the goal position $[x_g, y_g]$, whereas s_T is the distance between the prediction final position $[x(T_p), y(T_p)]$ and $[x_g, y_g]$. Visual representations of these variables are shown in Fig. 2b. ψ_{diff} is the difference between the final heading angle $\psi(T_p)$ and the angle of the $[x_g, y_g]$ relative to $[x(T_p), y(T_p)]$, which is calculated as

$$\psi_{\text{diff}} = \text{atan2}\left[\sin(\psi(T_p) - \psi_{\text{frg}}), \cos(\psi(T_p) - \psi_{\text{frg}})\right] \tag{27}$$

$$\psi_{\text{frg}} = \text{atan2}\left[y_g - y(T_p), x_g - x(T_p)\right] \tag{28}$$

T_p is the prediction horizon. If proper weighting factors are selected, the first three terms will result in a trajectory in which the end point of the predicted trajectory is close to the target, the final heading angle is pointing to the target, and the time used to cover the prediction distance is small.

Furthermore, three integral terms are included in the cost function. The first term, I_1, penalizes the cost when the tire vertical load is close to the specified threshold, which is used to prevent vehicle from operating at the limit unnecessarily. The second term, I_2, is used to minimize the integral over the prediction horizon of the distance to the line that is passing through the goal $[x_g, y_g]$ along a desired direction ϕ_g. This term is used to have the vehicle pass through the target from the desired direction. The third term, I_3, is a regularization term minimizing the control effort that is defined as the integral of the weighted sum of δ_f^2, ς_f^2, and J_x^2.

$$I_1 = \int_0^{T_p} \left\{2 + \tanh\left[-(F_{z,rl} - a)/b\right] + \tanh\left[-(F_{z,rr} - a)/b\right]\right\} \mathrm{d}t \tag{29}$$

$$I_2 = \int_0^{T_p} \left\{\sin(\phi_g)\left[x(t) - x_g\right] - \cos(\phi_g)\left[y(t) - y_g\right]\right\}^2 \mathrm{d}t \tag{30}$$

$$I_3 = \int_0^{T_p} \left[\varsigma_f^2(t) + w_\delta \delta_f^2(t) + w_J J_x^2(t)\right] \mathrm{d}t \tag{31}$$

This completes the description of the formulation.

3.8 Solving the OCP

The resulting OCP problem is solved using a pseudo-spectral method to transform the continuous-time optimization problem into a nonlinear programming problem [28], which is then solved using the interior point method [29].

4 SIMULATION RESULTS AND DISCUSSION

In this section, numerical simulations of the developed nonlinear MPC obstacle avoidance algorithm with the 14 DoF vehicle model mentioned in Section 3.1 as the AGV shown in Fig. 1 are presented.

Two scenarios are considered with two different obstacle fields, and each scenario is simulated with both the formulation presented in this paper and the constant speed formulation of [19] for comparison. All simulations are run with a vehicle initial speed of 20 m/s. The LIDAR detection range is $R_{\text{LIDAR}} = 100$ m. The goal is to pass through the specified target from the 90 degrees direction in the global coordinate. At each step of the MPC, the optimization generates a trajectory within the 100 m LIDAR detection range. Only the first 0.5 second of the planned control command is executed by the vehicle. A new trajectory is planned every 0.5 second using the updated vehicle state information and obstacle information from the sensors.

The results of the first scenario are shown in Fig. 13. In this case, both the constant speed algorithm and variable speed algorithm navigate the vehicle through the obstacle field safely; i.e., collision-free as shown in Fig. 13a and without tire lift-off as shown in Fig. 13d and Fig. 13e. In the constant speed case, because the speed controller used does not take the steering input into account, the speed has a maximum deviation of 0.3 m/s from the desired value of 20 m/s. In the variable speed case, the speed of the vehicle gradually increases from 20 m/s up to 22 m/s and decreases back towards 20 m/s within the final 3.5 seconds as desired. In this case, the vehicle arrives the target 1.7 seconds earlier out of the 25 seconds trajectory; i.e., about 7% faster.

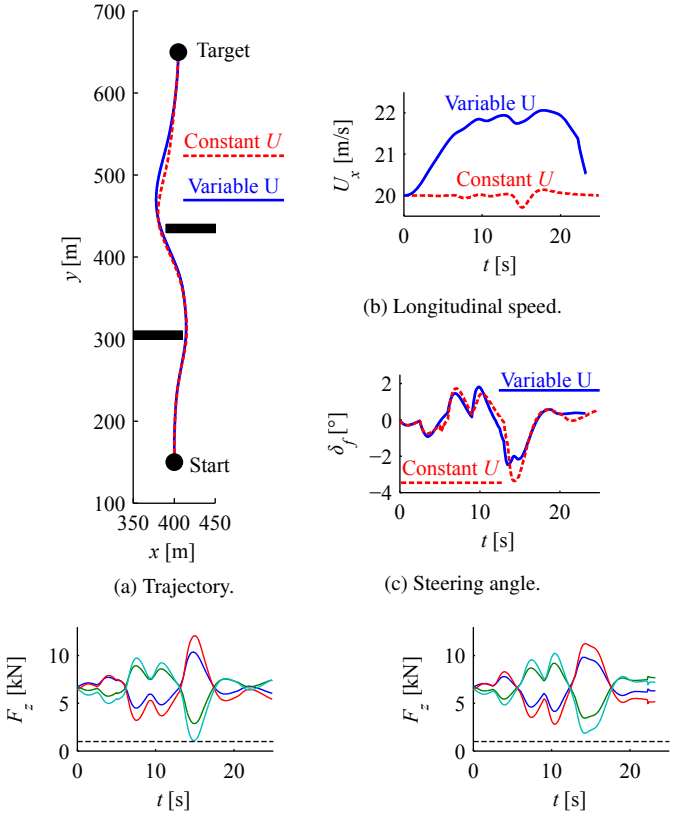

(a) Trajectory. (b) Longitudinal speed. (c) Steering angle. (d) Vertical load for the constant speed case. (e) Vertical load for the variable speed case.

FIGURE 13. Results of simulation set 1. Both constant speed and variable speed navigations are successful. In the variable speed case, the vehicle arrives the target earlier. In the subplots (d) and (e), the black dashed lines indicate the minimum allowable vertical tire force.

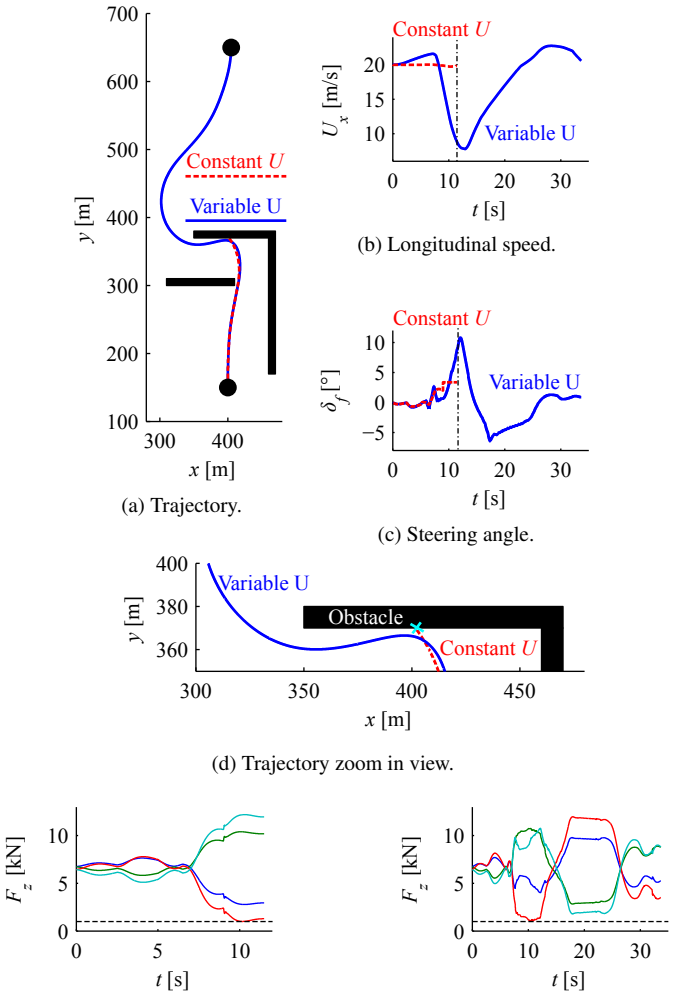

(a) Trajectory. (b) Longitudinal speed. (c) Steering angle. (d) Trajectory zoom in view. (e) Vertical load for the constant speed case. (f) Vertical load for the variable speed case.

FIGURE 14. Results of simulation set 2. The constant speed navigation fails while the variable speed navigation is successful.

A more important benefit of the new formulation is demonstrated with the second scenario as shown in Fig. 14. With the constant speed algorithm, the vehicle collides with the obstacle after 11.5 seconds. However, with the variable speed algorithm, the vehicle is safely navigated through the obstacle field by decelerating to a speed around 10 m/s. The vehicle starts accelerating again after the obstacle is cleared. As shown in Fig. 14a and Fig. 14d, the trajectory is collision free. Fig. 14f shows that the tire vertical loads are all above the specified threshold; hence, dynamical safety of the vehicle is ensured, as well.

5 SUMMARY AND CONCLUSIONS

This paper considers AGVs in unstructured environments without *a priori* information about the obstacles and presents an MPC-based obstacle avoidance algorithm that optimizes the longitudinal speed and steering angle simultaneously to navigate the AGV safely and as quickly as possible to the target location. A multi-stage OCP formulation is used to incorporate the obstacle data obtained from the on-board LIDAR sensor. The formulation of the OCP to be solved at each step of the MPC is discussed in detail. The powertrain and brake dynamics are taken into consideration through the bounds on vehicle longitudinal speed, acceleration and jerk. The dynamical safety requirement is also accounted for by enforcing a positive vertical load on all four tires. Two sets of numerical simulations are conducted to demonstrate the effectiveness of the algorithm. The conclusion is that the developed variable speed algorithm not only improves the performance of the vehicle by allowing it to operate closer to its dynamical limits, but also enables the safe clearance of obstacle fields that may not be cleared with steering control alone.

Future research directions include investigation of alternative cost function formulations and systematic ways of selecting the weighting factors. Incorporation of uncertainties in the model and sensor measurements is another direction. Although the prediction-correction characteristic allows the algorithm to tolerate some errors and uncertainties, incorporating them explicitly would further increase the robustness of the algorithm. Finally, extension of the formulation to moving obstacles is also an important direction for future research.

ACKNOWLEDGMENT

The authors wish to acknowledge the financial support of the Automotive Research Center (ARC) in accordance with Cooperative Agreement W56HZV-14-2-0001 U.S. Army Tank Automotive Research, Development and Engineering Center (TARDEC) Warren, MI.

REFERENCES

[1] S. M. LaValle, *Planning algorithms*, Cambridge University Press, 2006.

[2] B. D. Luders, S. Karaman, and J. P. How, "Robust sampling-based motion planning with asymptotic optimality guarantees," in *Proceedings of the AIAA Guidance, Navigation, and Control Conference (GNC)*, 2013.

[3] O. Khatib, "Real-time obstacle avoidance for manipulators and mobile robots," *International Journal of Robotics Research*, vol. 5, pp. 90-98, 1986.

[4] S. Shimoda, Y. Kuroda, and K. Iagnemma, "High-speed navigation of unmanned ground vehicles on uneven terrain using potential fields," *Robotica*, vol. 25, pp. 409-424, 2007.

[5] A. Hussein, H. Mostafa, M. Badrel-Din, O. Sultan, and A. Khamis, "Meta-heuristic optimization approach to mobile robot path planning," in *Proceedings of the International Conference on Engineering and Technology (ICET)*, 2012.

[6] P. Ogren and N. E. Leonard, "A convergent dynamic window approach to obstacle avoidance," *IEEE Transactions on Robotics*, vol. 21, pp. 188-195, 2005.

[7] Y. Gao, T. Lin, F. Borrelli, E. Tseng, and D. Hrovat, "Predictive control of autonomous ground vehicles with obstacle avoidance on slippery roads," in *Proceedings of the Dynamic Systems and Control Conference (DSCC)*, 2010.

[8] J. M. Park, D. W. Kim, Y. S. Yoon, H. J. Kim, and K. S. Yi, "Obstacle avoidance of autonomous vehicles based on model predictive control," *Proceedings of the Institution of Mechanical Engineers, Part D: Journal of Automobile Engineering*, vol. 223, pp. 1499-1516, 2009.

[9] G. P. Bevan, H. Gollee, and J. O'Reilly, "Trajectory generation for road vehicle obstacle avoidance using convex optimization," *Proceedings of the Institution of Mechanical Engineers, Part D: Journal of Automobile Engineering*, vol. 224, pp. 455-473, 2010.

[10] A. Tahirovic and G. Magnani, "General framework for mobile robot navigation using passivity-based MPC," *IEEE Transactions on Automatic Control*, vol. 56, pp. 184-190, 2011.

[11] A. Gray, Y. Gao, T. Lin, J. K. Hedrick, H. E. Tseng, and F. Borrelli, "Predictive control for agile semi-autonomous ground vehicles using motion primitives," in *Proceedings of the American Control Conference (ACC)*, 2012, pp. 4239-4244.

[12] J. V. Frasch, A. Gray, M. Zanon, H. J. Ferreau, S. Sager, F. Borrelli, and M. Diehl., "An auto-generated nonlinear MPC algorithm for real-time obstacle avoidance of ground vehicles," in *Proceedings of the European Control Conference (ECC)*, 2013.

[13] J. H. Jeon, R. V. Cowlagi, S. C. Peters, S. Karaman, E. Frazzoli, P. Tsiotras, and K. Iagnemma, "Optimal motion planning with the half-car dynamical model for autonomous high-speed driving," in *Proceedings of the American Control Conference (ACC)*, 2013, pp. 188-193.

[14] P. Falcone, F. Borrelli, J. Asgari, H. E. Tseng, and D. Hrovat, "A model predictive control approach for combined braking and steering in autonomous vehicles," in *Proceedings of the Mediterranean Conference on Control and Automation (MED)*, 2007, pp. 1-6.

[15] S. J. Anderson, S. C. Peters, T. E. Pilutti, and K. Iagnemma, "An optimal-control-based framework for trajectory planning, threat assessment, and semi-autonomous control of passenger vehicles in hazard avoidance scenarios," *International Journal of Vehicle Autonomous Systems*, vol. 8, pp. 190-216, 2010.

[16] A. Gray, M. Ali, Y. Gao, J. K. Hedrick, and F. Borrelli, "A unified approach to threat assessment and control for automotive active safety," *IEEE Transactions On Intelligent Transportation Systems*, vol. 14, pp. 1490-1499, 2013.

[17] C. E. Beal and J. C. Gerdes,"Model predictive control for vehicle stabilization at the limits of handling", *IEEE Transactions on Control Systems Technology*, vol. 21, pp. 1258-1269, 2013.

[18] J. Liu, P. Jayakumar, J. L. Overholt, J. L. Stein, and T. Ersal, "The role of model fidelity in model predictive control based hazard avoidance in unmanned ground vehicles using LIDAR sensors", in *Dynamic Systems and Control Conference (DSCC)*, 2013.

[19] J. Liu, P. Jayakumar, J. L. Stein, and T. Ersal, "A multi-stage optimization formulation for mpc-based obstacle avoidance in autonomous vehicles using a LIDAR sensor", in *Dynamic Systems and Control Conference (DSCC)*, 2014.

[20] H. B. Pacejka, *Tire and vehicle dynamics*, Elsevier, 2005.

[21] A. Rucco, G. Notarstefano, and J. Hauser, "Optimal control based dynamics exploration of a rigid car with longitudinal load transfer", *IEEE Transactions on Control Systems Technology*, 22(3), pp. 1070-1077, 2014.

[22] T. Shim and C. Ghike, "Understanding the limitations of different vehicle models for roll dynamics studies", *Vehicle System Dynamics*, vol. 45, pp. 191-216, 2007.

[23] D. N. Assanis, Z. Filipi, S. Gravante, D. Grohnke, X. Gui, L. Louca, G. Rideout, J. L. Stein, and Y. Wang, "Validation and use of Simulink integrated, high fidelity, engine-in-vehicle simulation of the international class VI truck", *SAE Technical Paper*, No. 2000-01-0288, 2000.

[24] T. Ersal, M. Brudnak, A. Salvi, J. L. Stein, Z. Filipi, and H. K. Fathy,"Development and model-based transparency analysis of an Internet-distributed hardware-in-the-loop simulation platform", *Mechatronics*, 21(1), pp. 22-29, 2011.

[25] K. Hedrick, J. C. Gerdes, D. B. Maciuca, and D. Swaroop, "Brake System Modeling, Control And Integrated Brake/throttle Switching Phase I", *California Partners for Advanced Transit and Highways (PATH)*, 1997.

[26] B. C. Chen, and H. Peng, "Rollover warning for articulated heavy vehicles based on a time-to-rollover metric", *Journal of Dynamic Systems, Measurement and Control*, vol. 127, pp. 406-414, 2005.

[27] S. Rakheja, and A. Piche, "Development of directional stability criteria for an early warning safety device", *SAE Technical Paper*, No. 902265, pp. 877-889, 1990.

[28] C. L. Darby, W. W. Hager, and A. V. Rao, "An hp-adaptive pseudospectral method for solving optimal control problems", *Optimal Control Applications and Methods*, vol. 32, pp. 476-502, 2011.

[29] A. Waechter and L. T. Biegler, "On the implementation of an interior-point filter line-search algorithm for large-scale nonlinear programming", *Mathematical Programming*, vol. 106, pp. 25-57, 2006.